Journal of Alloys and Compounds 807 (2019) 151675

Contents lists available at ScienceDirect

Journal of Alloys and Compounds

journal homepage: http://www.elsevier.com/locate/jalcom

Effects of Ho addition on thermal stability, thermoplastic deformation and magnetic properties of FeHoNbB bulk metallic glasses

Feng Hu [a], Chenchen Yuan [a, *], Qiang Luo [a], Weiming Yang [b], Baolong Shen [a, b, **]

[a] School of Materials Science and Engineering, Jiangsu Key Laboratory for Advanced Metallic Materials, Southeast University, Nanjing, 211189, China
[b] Institute of Massive Amorphous Metal Science, China University of Mining and Technology, Xuzhou, 221116, China

ARTICLE INFO

Article history:
Received 17 May 2019
Received in revised form
17 July 2019
Accepted 1 August 2019
Available online 2 August 2019

Keywords:
Fe-based BMGs
Thermoplastic formability
Glass-forming ability
Soft magnetic properties

ABSTRACT

The influences of Ho addition on the thermal stability of supercooled liquids, thermoplastic deformation as well as mechanical and soft-magnetic behaviors of $Fe_{71-x}Ho_xNb_6B_{23}$ bulk metallic glasses (BMGs) were investigated. With increasing Ho content from 1 to 5 at. %, the supercooled liquid region (SCLR) increased from 48 to 90 K, and the thermal stability is largely enhanced through remained chemical short- or medium-ordering. Combined with the competitive formation process of the complex $Fe_{23}B_6$ and $Ho_2Fe_{14}B$ phases, the glass-forming ability (GFA) of the alloy system was improved, allowing for the fabrication of glassy rods up to 3 mm in diameter. Due to the large SCLR and GFA, the $Fe_{66}Ho_5Nb_6B_{23}$ BMG with high fracture strength of 3.45 GPa shows outstanding thermoplastic forming ability accompanied with good soft magnetic performance.

1. Introduction

Bulk metallic glasses (BMGs) have attracted great research interest due to their many excellent properties and potential for applications [1]. As one of the potential applications, micro-parts of Zr-based BMGs have been successfully prepared by thermoplastic deformation utilizing their viscous flow workability [2,3]. Compared with Zr-based BMGs, the micro-parts made of thermoplastic deformed Fe-based BMGs are more potential for future applications as micro-devices because they have superhigh strength, excellent soft-magnetic properties and high corrosion resistance [4–9]. BMGs for the thermoplastic processing should simultaneously possess a large supercooled liquid region (SCLR) and excellent glass-forming ability (GFA) [10]. However, there are few reports on thermoplastic deformation of Fe-based BMGs, due to their small SCLR and low GFA [11–13]. On the other hand, it has been confirmed that rare-earth (RE) elements are effective to improve the thermal stability of supercooled liquid and GFA of Fe- and Co-based BMGs [14–17], because RE elements can suppress the precipitation of metastable $Fe_{23}B_6$ and α-Fe crystalline phases [18], leading to the improvement of SCLR and GFA. One of Co-based BMGs containing RE element of Dy with large SCLR of 110 K and superhigh strength of 4.75 GPa has been successfully prepared and thermoplastic deformed [19].

In this study, with the purpose of developing a thermoplastic-deformable Fe-based BMG with superhigh strength and good soft-magnetic properties, we focused on $Fe_{71}Nb_6B_{23}$ glassy alloy because it exhibits a superhigh fracture strength (σ_f) as high as 4.85 GPa [20], which is the strongest Fe-based BMG with good soft-magnetic performances, however, this FeNbB ternary alloy can be only fabricated into glassy rod with a critical diameter (D_C) of 1.5 mm and exhibits a small SCLR of 40 K [13]. Therefore, it is necessary to improve the SCLR and GFA for thermoplastic deformation of this alloy without severely decreasing its superhigh strength and soft-magnetic properties. Recently, we have successfully prepared FeErBNb bulk glassy alloys with improved GFA and tunable Curie temperature by adding Er to $Fe_{71}Nb_6B_{23}$ alloy [21]. Therefore, according to this result, we tried to substitute Fe with RE element of Ho with the aim at preparing FeHoNbB glassy alloys with large GFA and SCLR, and the effect of the Ho element on the GFA and thermal stability of supercooled liquid were also investigated. As a result, it was found that 5 at. % Ho addition is effective to improve the thermal stability of supercooled liquid and the GFA. The $Fe_{66}Ho_5Nb_6B_{23}$ bulk glassy rod with a diameter of 3 mm and a large SCLR of 90 K was prepared, which shows superhigh strength, good soft-magnetic properties. The large SCLR and high GFA made $Fe_{66}Ho_5Nb_6B_{23}$ glassy alloy possible for the application of

* Corresponding author.
** Corresponding author. School of Materials Science and Engineering, Southeast University, Nanjing, 211189, China.
E-mail addresses: yuancc@seu.edu.cn (C. Yuan), blshen@seu.edu.cn (B. Shen).

https://doi.org/10.1016/j.jallcom.2019.151675
0925-8388/

thermoplastic deformation.

2. Experimental

The ribbons with nominal compositions of $Fe_{71-x}Ho_xNb_6B_{23}$ ($0 \le x \le 6$) were produced by single roller melt-spinning. Glassy rods with different diameters up to 3 mm were fabricated by copper-mold casting method. The glassy structure and thermal behaviors of the samples were measured by X-ray diffraction (XRD, Bruker D8 Discover diffractometer) with Cu Kα radiation and differential scanning calorimetry (DSC, NETZSCH 404 F3) at a heating rate of 0.67 K/s, respectively. Samples for crystallization behavior were annealed at the pressure of 2×10^{-3} Pa for 600s in the annealing furnace. The crystalline phases were examined by XRD. The glassy specimens were also annealed at different temperatures in DSC and annealing furnace within the SCLR to observe exothermic peak. Magnetic flux density (B_s) of samples were measured by vibrating sample magnetometer (VSM, Lake Shore 7410) in the magnetic field up to 800 kA/m. Coercivity (H_c) was measured with a *DC B*−*H* loop tracer (RIKEN BHS-40) under a magnetic field of 1000 A/m. The compressive fracture strengths (σ_f) at both room temperature and the high temperature were measured on 1×2 mm glassy rods with a compressive strain rate of 5×10^{-4} s^{-1} by the testing machine (CMT 4503). Vickers hardness (H_v) was measured by a hardness tester (FM-700) under a load of 9.8 N. Five samples for each component were used for both σ_f and H_v measurements. Thermoplastic deformation was performed at a temperature interval within SCLR also using the testing machine (CMT 4503). The microstructures of samples before and after annealing were examined by transmission electron microscopy (TEM, JEM2000ex).

3. Results and discussion

Fig. 1 shows DSC curves of the $Fe_{71-x}Ho_xNb_6B_{23}$ ($0 \le x \le 6$) glassy ribbons. Compared with $Fe_{71}Nb_6B_{23}$ glassy alloy, each Ho-containing alloy exhibits an obvious glass transition followed with a large SCLR as shown in the figure. With increasing Ho content from 0 to 5 at. %, glass transition temperature (T_g) and crystallization temperature (T_x) increase gradually from 824 to 885 K and 863−975 K, respectively, resulting in an increase of SCLR ($\Delta T_x = T_x - T_g$) from 39 to 90 K. However, with further increasing Ho content to 6 at. %, although T_g increases to 908 K, T_x keeps at 975 K, causing the decrease of SCLR from 90 to 70 K. This indicates that 5 at. % Ho addition is the most effective to improve the thermal stability of supercooled liquid in this Fe-based glassy alloy system. Besides, it is interesting to notice that the main exothermic peak (marked as P_1) splits into two peaks with increasing Ho content from 3 to 6 at. %. The intensity of second exothermic peak (marked as P_2) increases gradually, which becomes dominant with increasing Ho content. For the alloys containing 5 and 6 at. % Ho, the P_2 peak is even stronger than the P_1 peak, and the P_1 peak of the alloy with 5 at. % Ho was covered by P_2 peak, only remaining a shoulder-like peak in the curve (marked as P_{sho}). With further increasing Ho content to 6 at. %, the P_{sho} peak is separated as an independent peak. Meanwhile, an exothermic peak marked as P_0 in the SCLR can be observed for the alloys with 4, 5, and 6 at. % Ho additions. The temperature corresponding to P_0 is defined as T_{inf}. The P_0 peak appearing in the 4 at. % Ho-containing alloy decreases gradually with further increasing Ho content to 5 and 6 at. %, the detailed reason will be discussed later. Anyway, the SCLR increases to the largest value of 90 K with 5 at. % Ho addition.

As described above, the thermal stability of the supercooled liquid of this alloy system was drastically affected by the Ho content. To study the reason why Ho addition has a high effect for improving the thermal stability of the supercooled liquid, the change of crystallization phases of the FeHoNbB glassy alloys with 5 and 6 at. % Ho was investigated in detailed. Figs. 2 and 3 respectively show XRD patterns of the $Fe_{66}Ho_5Nb_6B_{23}$ and $Fe_{65}Ho_6Nb_6B_{23}$ glassy alloys annealed at different temperatures for 600 s. First, as shown in Fig. 2, it is noteworthy that the XRD pattern shows the $Fe_{66}Ho_5Nb_6B_{23}$ glassy alloy annealed at the temperature of P_0 peak ($T_{inf} = 943$ K) almost kept the amorphous structure, indicating the high thermal stability of supercooled liquid, which is very beneficial for thermoplastic deformation. When the annealing temperature increases to 973 K, just lower than the onset temperature of the P_{sho} peak for the $Fe_{66}Ho_5Nb_6B_{23}$ sample, the precipitation phases are $Fe_{23}B_6$ and $Ho_2Fe_{14}B$. It has been reported that the primary crystallization phase for the $Fe_{71}Nb_6B_{23}$ sample is the metastable $Fe_{23}B_6$ phase [13]. However, in this study, the primary precipitation phases are $Fe_{23}B_6$ and $Ho_2Fe_{14}B$ phases for the $Fe_{66}Ho_5Nb_6B_{23}$ glassy alloy. For the $Fe_{65}Ho_6Nb_6B_{23}$ glassy alloy, as shown in Fig. 3, the precipitation phase is only $Ho_2Fe_{14}B$ phase as the sample annealed at the same temperature of 973 K, which means the primary precipitation phase changes from $Fe_{23}B_6$ and $Ho_2Fe_{14}B$ two phases to one $Ho_2Fe_{14}B$ phase with increasing only 1 at. % Ho. When the annealing temperature increases to 1003 K for the $Fe_{65}Ho_6Nb_6B_{23}$ glassy alloy, which is the finishing temperature of the P_{sho} peak and the onset temperature of P_2 peak as shown in Fig. 1, the precipitation phases are $Ho_2Fe_{14}B$ and α-Fe phases. So that it is considered that the P_{sho} is due to the precipitation of $Fe_{23}B_6$ and $Ho_2Fe_{14}B$ phases for the $Fe_{66}Ho_5Nb_6B_{23}$ glassy alloy, and corresponding to the precipitation of $Ho_2Fe_{14}B$ phase for the

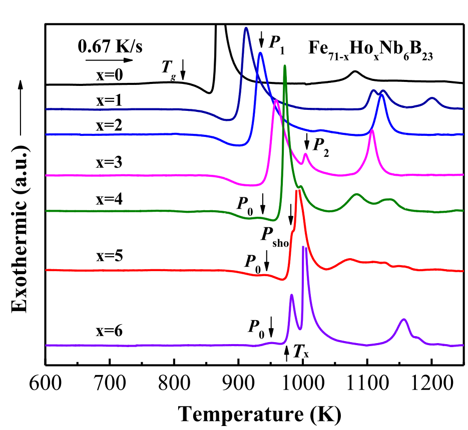

Fig. 1. DSC curves of melt-spun $Fe_{71-x}Ho_xNb_6B_{23}$ ($0 \le x \le 6$) glassy ribbons.

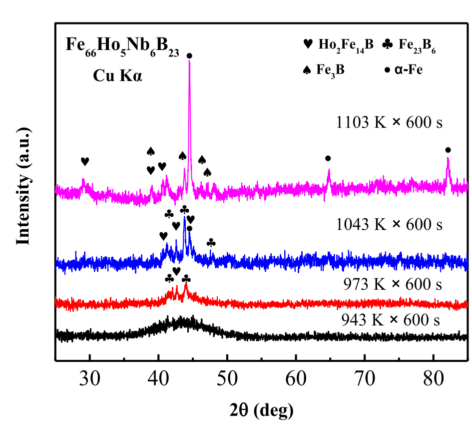

Fig. 2. XRD patterns of $Fe_{66}Ho_5Nb_6B_{23}$ ribbons at different annealing temperatures.

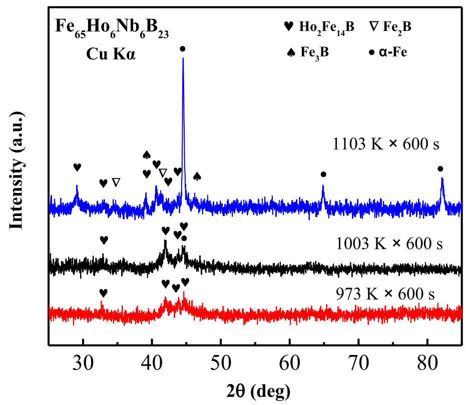

Fig. 3. XRD patterns of $Fe_{65}Ho_6Nb_6B_{23}$ ribbons at different annealing temperatures.

$Fe_{66}Ho_6Nb_6B_{23}$ glassy alloy. The P_2 peak is the exothermic peak corresponding to the precipitation of the α-Fe phase. Therefore, it can be concluded that the primary precipitation phase of this FeHoNbB glassy alloy system is single $Fe_{23}B_6$ phase for 0–3 at. % Ho-containing alloys, and changes to $Fe_{23}B_6$ and $Ho_2Fe_{14}B$ two phases for 4 and 5 at. % Ho-containing alloy, then becomes a single $Ho_2Fe_{14}B$ phase for 6 at. % Ho-containing alloy. It has been reported that the competitive formation of $Fe_{23}B_6$ and $Ho_2Fe_{14}B$ phases can improve the GFA, because the precipitation of both $Fe_{23}B_6$ and $Ho_2Fe_{14}B$ competing crystalline phases requires long-range atomic rearrangement, thus the atomic diffusion becomes more difficult, leading to the improvement of GFA [22,23].

Based on the results mentioned above, we tried to prepare BMG samples, the glassy rods of $Fe_{71-x}Ho_xNb_6B_{23}$ ($1 \le x \le 6$) alloy were synthesized with critical diameters up to 3 mm, the XRD curves of which are shown Fig. 4. Only broad peaks are seen in XRD patterns for these BMGs, indicating the fully glassy structure. The D_C is 1, 1.5, 2, 2.5, 3, and 1.5 mm respectively for the $Fe_{71-x}Ho_xNb_6B_{23}$ glassy alloys with 1–6 at. % Ho addition. The largest critical size is 3 mm for the 5 at. % Ho-containing alloy, which is consistent with the analysis of thermal stability of the supercooled liquid according to DSC and XRD measurements. Besides, it is seen that the peak position (2θ) of the principal diffraction hump gradually decreases from 45.1 to 43.9° with increasing Ho content (as shown by the black arrow in the figure), indicating that the local atomic structure changes with Ho addition [24].

It is known that large GFA and SCLR are necessary for the thermoplastic deformation of bulk glassy alloy [19,25]. In this study, the $Fe_{66}Ho_5Nb_6B_{23}$ glassy alloy rod can be prepared with the D_C of 3 mm and exhibits a large SCLR of 90 K, which indicates that it is possible for thermoplastic deformation, but there is an exothermic peak P_o in SCLR, although the XRD pattern shows it keeps amorphous structure even after annealing at the P_o temperature of 943 K for 600 s as shown in Fig. 2. Therefore, it is necessary to further confirm whether the P_o is an exothermic peak caused by the precipitation of microstructure [26] or only results from chemical short- [18] or medium- [27] range ordering.

Fig. 5 shows DSC curves of $Fe_{71-x}Ho_xNb_6B_{23}$ (x = 4, 5, 6 at. %) glassy ribbons isothermally annealed for 120 s at the temperature of P_o. DSC curves of the as-quenched ribbons are also shown for comparison. Compared with as-quenched samples, it can be clearly seen that all P_o peaks of annealed samples disappeared completely. To further investigate the transformation of the exothermic peak P_o and whether the precipitation happened after annealing, calorimetric measurements at different temperatures by DSC and microstructure observations by TEM were performed for the $Fe_{66}Ho_5Nb_6B_{23}$ ribbon.

Fig. 6 shows DSC traces of $Fe_{66}Ho_5Nb_6B_{23}$ ribbons once heated up to 925 K (before the $T_{inf.}$) and 945 K (around the $T_{inf.}$), as well as that of the as-cast alloy for comparison. It can be found that the P_o peak gradually disappears, but no apparent evidence for the formation of crystalline phases is observed in the bright field images, as shown in electronic selected area diffraction patterns and TEM images as well as XRD curves of both as-cast and annealed specimens in Fig. 7 and the inset of Fig. 6. Therefore, it is considered that the structural relaxation with no crystallization occurred by structural rearrangement of the metastable configuration during annealing, which is similar to the reported results [18,27,28]. The indirect evidence for structural rearrangement is the slight increase of T_g, which may be caused by the change of the chemical and topological short- and medium-range ordering [29,30]. The alloys which show P_o usually have a large SCRL [29,31], therefore, the thermal stability of the SCRL has a strong correlation with remained chemical short- or medium-ordering.

Considering the large SCLR and the exclusion of crystallization in the SCLR, the thermoplastic forming behavior of $Fe_{66}Ho_5Nb_6B_{23}$ BMG was conducted to explore their superplastic-flow ability. Fig. 8 shows the temperature dependence of strength for as-cast $Fe_{66}Ho_5Nb_6B_{23}$ glassy rod. The glassy rod exhibits a σ_f of 3.42 GPa and elastic strain followed by a disastrous fracture at room temperature. Whereas, the compression strength dramatically decreases accompanied by an overshoot as is often observed during homogeneous deformation in the supercooled liquid state [32], when the temperature rises above T_g (~883 K). Then the sample attains steady plastic flow at a strain rate 5×10^{-4} s^{-1}, which is a typical feature of homogeneous flow. With further increase of the testing temperature from 883 to 933 K, σ_f decreases obviously to

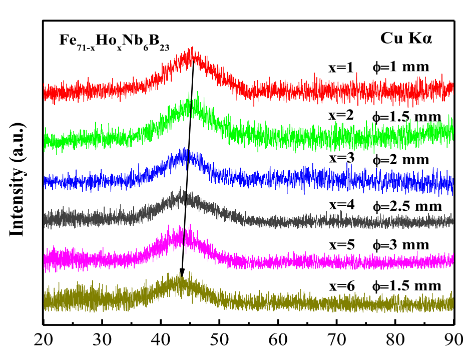

Fig. 4. XRD patterns of $Fe_{71-x}Ho_xNb_6B_{23}$ ($1 \le x \le 6$) glassy rods with critical diameters of 1, 1.5, 2, 2.5, 3, and 1.5 mm, respectively.

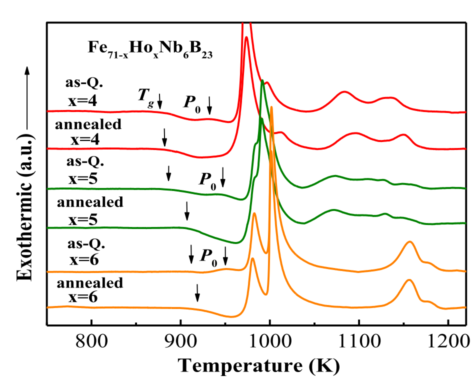

Fig. 5. DSC curves of both as-quenched and isothermally annealed for 120 s of $Fe_{71-x}Ho_xNb_6B_{23}$ ribbons samples (x = 4, 5, 6 at. %).

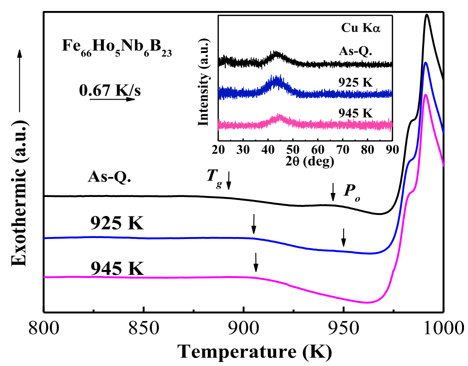

Fig. 6. DSC curves of the $Fe_{66}Ho_5Nb_6B_{23}$ samples annealed at various temperatures. The inset figure shows XRD patterns of the annealed samples.

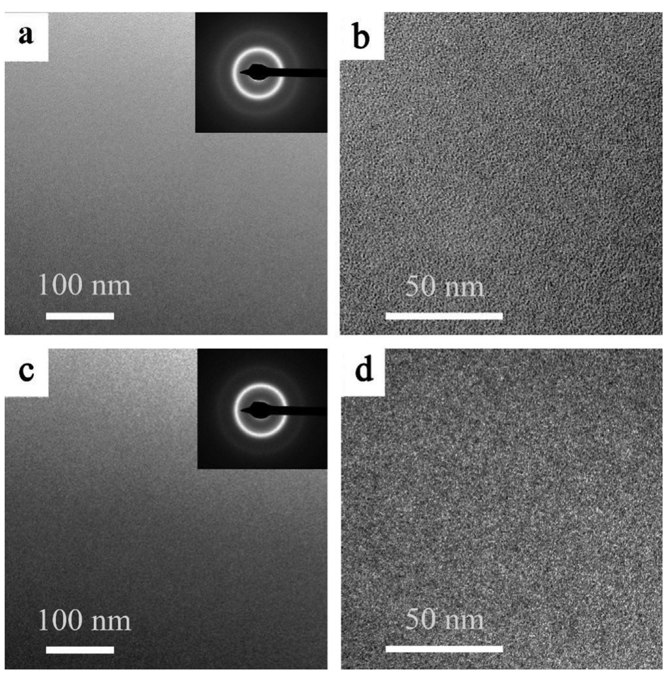

Fig. 7. TEM images obtained from the $Fe_{66}Ho_5Nb_6B_{23}$ ribbons in the as-melt spun state: (a) and (b). TEM images of the $Fe_{66}Ho_5Nb_6B_{23}$ ribbons once heated up to 945 K: (c) and (d).

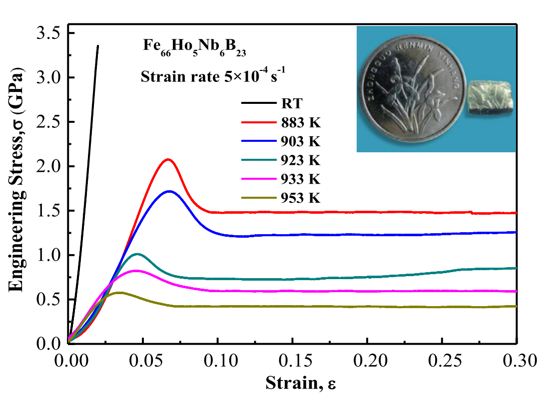

Fig. 8. The compressive stress-strain curves of 1 mm $Fe_{66}Ho_5Nb_6B_{23}$ as-cast rods at different temperatures. The inset figure shows the pattern of a Chinese dime coin imprinted into the $Fe_{66}Ho_5Nb_6B_{23}$ BMG sheet at 953 K.

below 0.08 GPa, lower than that of conventional steels [33]. The $Fe_{66}Ho_5Nb_6B_{23}$ 3 mm glassy rod was embossed with the pattern of a Chinese dime coin at 953 K under a pressure of 0.03 GPa, as shown in the inset of Fig. 8. The $Fe_{66}Ho_5Nb_6B_{23}$ BMG sample demonstrates a good thermoplastic-forming ability in the SCLR, displaying a total homogeneous plastic flow behavior at the strain rate of 5×10^{-4} s^{-1}. The mechanical performances of $Fe_{71-x}Ho_xNb_6B_{23}$ ($0 \le x \le 6$) glassy alloys at room temperature are also investigated and included in Table 1.

The soft magnetic properties of $Fe_{71-x}Ho_xNb_6B_{23}$ ($0 \le x \le 6$) ribbons are shown in Fig. 9. It can be seen that magnetic flux density (B_s) rapidly saturates in the external magnetic field, which exhibits good soft magnetic properties. However, due to the anti-ferromagnetic coupling between Fe and newly introduced Ho element [17,34,35], the contribution of noncolinear magnetic moment alignment is enhanced [35,36], which leads to the B_s decreases gradually from 1.09 to 0.45 T with increasing Ho content from 1 to 6 at. %. It is noteworthy that the H_c of this alloy system increases with Ho addition as shown by the blue line in Fig. 10. It is known the total H_c in the glassy alloy can be expressed as [37,38]:

$$H_c = H_c^{surf} + H_c^{\sigma} + H_c^{so} + H_c^{rel} + H_c^{i} \tag{1}$$

where H_c^{surf}, H_c^{σ}, H_c^{so}, H_c^{rel} and H_c^{i} originate from surface roughness, magnetoelastic coupling, directional short-range ordering of atom pairs, structure relaxation, and intrinsic fluctuations of exchange energies, respectively. It can be assumed that H_c^{surf},H_c^{rel} and H_c^{i} have a very small contribution with the change of composition. According to the Bragg equation (2)$r_1 \sin\theta = \lambda$, the maximum halo scatter angle 2θ is in connection with the average radius of the first coordination shell r_1. Thus, from the XRD results as shown in Fig. 4, it is concluded that the r_1 of the $Fe_{71-x}Ho_xNb_6B_{23}$ glassy alloys increases with increasing Ho content. Replacement of shell Fe (0.126 nm) atoms by the large radius of Ho (0.176 nm) atoms may raise the distortion and local anisotropy of atomic clusters, leading to an increase of H_c^{so}. On the other hand, it is reported that doping RE can enhance the saturation magnetostriction (λ_s) of Fe-based glassy alloy [39], and H_c^{σ} usually has a positive correlation with λ_s [38,40]:

$$H_c^{\sigma} \approx |\sigma \lambda_s| / |M_s| \tag{2}$$

where M_s is the saturation magnetization. Therefore, the total H_c increases with the increase of Ho content. In addition, the r_1 increasing with Ho addition also indicates that the bonds of the nearest neighbor atoms are weakened by Ho addition. This may be the reason that the strength of this alloy system decreases with Ho addition as shown in Fig. 10. The RE-bearing BMGs usually show a high flaw sensitivity and appear premature fracture tends before reaching their intrinsic material strength [41], which may be another reason for the descending compression strength and hardness with increasing Ho content.

Table 1 summarizes comprehensive performance of the $Fe_{71-x}Ho_xNb_6B_{23}$ ($0 \le x \le 6$) alloy system. The average values of mechanical properties are measured by using five samples for each composition. It can be found that the composition presenting the best comprehensive performance is $Fe_{66}Ho_5Nb_6B_{23}$, which not only has a large SCLR of 90 K, but also exhibits a maximum critical size of 3 mm in diameter. Meanwhile, this alloy system exhibits reasonably good magnetic and mechanical properties.

4. Conclusions

The influences of Ho addition on comprehensive properties of $Fe_{71-x}Ho_xNb_6B_{23}$ ($0 \le x \le 6$) glassy alloy system were investigated.

Table 1
The data of D_C, T_g, T_x, $\triangle T_x$, B_s, H_c, σ_f, and H_v of $Fe_{71-x}Ho_xNb_6B_{23}$ ($0 \le x \le 6$) glassy alloys.

Alloy	Dc	Thermal stability			Magnetic properties		Mechanical properties	
	Φ (mm)	T_g (K)	T_x (K)	$\triangle T_x$ (K)	B_s (T)	H_c (A/m)	σ_f (GPa)	H_v (kg/mm^2)
$Fe_{71}Ho_0Nb_6B_{23}$	1	824	863	39	1.09	3.39	4.65	1090
Fe70Ho1Nb6B23	1	849	897	48	0.99	4.46	4.25	1065
$Fe_{69}Ho_2Nb_6B_{23}$	1.5	864	919	55	0.84	6.55	4.10	1060
$Fe_{68}Ho_3Nb_6B_{23}$	2	871	943	72	0.68	7.27	3.96	1055
$Fe_{67}Ho_4Nb_6B_{23}$	2.5	880	964	84	0.61	9.56	3.75	1050
$Fe_{66}Ho_5Nb_6B_{23}$	3	886	975	90	0.51	11.28	3.42	1045
$Fe_{65}Ho_6Nb_6B_{23}$	1.5	908	976	68	0.45	9.97	3.15	1040

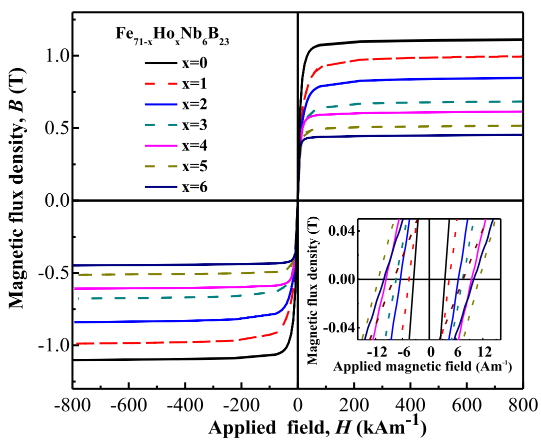

Fig. 9. B–H hysteresis curves of the annealed melt-spun $Fe_{71-x}Ho_xNb_6B_{23}$ ($0 \le x \le 6$) glassy ribbons measured by VSM. The insert is the enlarged B–H loop tracer.

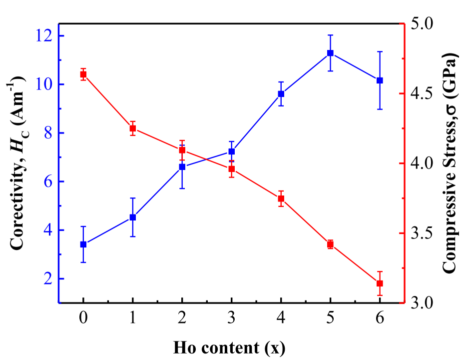

Fig. 10. The coercivity (left axis) and compressive stress (right axis) of $Fe_{71-x}Ho_xNb_6B_{23}$ ($0 \le x \le 6$) glassy alloys as a function of Ho content.

The results are summarized below:

(1) Doping 5 at. % Ho into $Fe_{71}Nb_6B_{23}$ glassy alloy effectively improves the GFA and thermal stability of the supercooled liquid, fabricating glassy alloy rod with a D_C of 3 mm in diameter and achieving a large SCLR of 90 K.
(2) The competitive formation of $Fe_{23}B_6$ and $Ho_2Fe_{14}B$ phases is beneficial for suppressing long-range atomic rearrangement, thus the atomic diffusion becomes more difficult, which leads to the improvement of GFA of $Fe_{66}Ho_5Nb_6B_{23}$.
(3) It was found the addition of 4–6 at. % Ho induces the unusual exothermic reaction in the SCLR of $Fe_{71-x}Ho_xNb_6B_{23}$ alloy. The structural relaxation with no crystallization occurred during annealing in the SCLR, indicating that P_o may be caused by structure transformation of chemical short- or medium-range order. When the compression temperature is above 933 K, it shows a good thermoplastic forming ability in the SCLR.
(4) These glassy rods also show a high saturation magnetic flux density of 1.09–0.45 T, a high σ_f of 4.65–3.15 GPa and a large Vickers hardness of 1090–1040 kg/mm^2, respectively. These excellent properties make the Fe-based alloys promising as structural materials.

Acknowledgements

This work was supported by the National Natural Science Foundation of China (Grant Nos. 51631003, 51601038 and 51601130), the National Key Research and Development Program of China (Grant No. 2016YFB0300502).

References

[1] W.H. Wang, C. Dong, C.H. Shek, Bulk metallic glasses, Mater. Sci. Eng. R 44 (2004) 45–89.
[2] J. Schroers, Processing of bulk metallic glass, Adv. Mater. 22 (2010) 1566–1597.
[3] G. Kumar, H.X. Tang, J. Schroers, Nanomoulding with amorphous metals, Nature 457 (2009) 868.
[4] M. Shi, S. Pang, T. Zhang, Towards improved integrated properties in FeCrPCB bulk metallic glassesby Cr addition, Intermetallics 61 (2015) 16–20.
[5] W.M. Yang, H.S. Liu, Y.C. Zhao, A. Inoue, K. Jiang, J.T. Huo, H.B. Ling, Q. Li, B.L. Shen, Mechanical properties and structural features of novel Fe-based bulk metallic glasses with unprecedented plasticity, Sci. Rep. 4 (2014) 6233.
[6] A.D. Wang, M.X. Zhang, J.H. Zhang, H. Men, B.L. Shen, S.J. Pang, T. Zhang, FeNiPBNb bulk glassy alloys with good soft-magnetic properties, J. Alloy. Comp. 536 (2012) S354–S358.
[7] A. Makino, T. Kubota, C.T. Chang, M. Makabe, A. Inoue, FeSiBP bulk metallic glasses with unusual combination of high magnetization and high glass-forming ability, Mater. Trans. 48 (2007) 3024–3027.
[8] X.J. Gu, A.G. McDermott, S.J. Poon, G.J. Shiflet, Critical Poisson's ratio for plasticity in Fe-Mo-C-B-Ln bulk amorphous steel, Appl. Phys. Lett. 88 (2006) 211905.
[9] V. Ponnambalam, S.J. Poon, G.J. Shiflet, V.M. Keppens, R. Taylor, G. Petculescu, Synthesis of iron-based bulk metallic glasses as nonferromagnetic amorphous steel alloys, Appl. Phys. Lett. 83 (2003) 1131–1133.
[10] J. Schroers, On the formability of bulk metallic glass in its supercooled liquid state, Acta Mater. 56 (2008) 471–478.
[11] A.D. Wang, Q.K. Man, M.X. Zhang, H. Men, B.L. Shen, S.J. Pang, T. Zhang, Effect of B to P concentration ratio on glass-forming ability and soft-magnetic properties in $[(Fe_{0.5}Ni_{0.5})_{0.78}B_{0.22-x}P_x]_{97}Nb_3$ glassy alloys, Intermetallics 20 (2012) 93–97.
[12] B.L. Shen, M. Akiba, A. Inoue, Effects of Si and Mo additions on glass-forming in FeGaPCB bulk glassy alloys with high saturation magnetization, Phys. Rev. B 73 (2006) 10424.
[13] J.H. Yao, H. Yang, J. Zhang, J.Q. Wang, The influence of Nb and Zr on glass-formation ability in the ternary Fe-Nb-B and Fe-Zr-B and quaternary Fe-(Nb, Zr)-B alloy systems, J. Mater. Res. 23 (2008) 392–401.
[14] Z. Han, J. Zhang, Y. Li, Quaternary Fe-based bulk metallic glasses with a diameter of 5mm, Intermetallics 15 (2007) 1447–1452.
[15] J.F. Li, Y. Shao, X. Liu, K.F. Yao, Fe-based bulk amorphous alloys with high glass formation ability and high saturation magnetization, Sci. Bull. 60 (2015) 396–399.
[16] D.H. Kim, J.M. Park, D.H. Kim, W.T. Kim, J. Mater. Res., Development of quaternary Fe-B-Y-Nb bulk glassy alloys with high glass-forming ability, J. Mater. Res. 22 (2007) 471–477.
[17] J.W. Li, A.N. He, B.L. Shen, Effect of Tb addition on the thermal stability, glass-forming ability and magnetic properties of Fe-B-Si-Nb bulk metallic glass, J. Alloy. Comp. 586 (2014) S46–S49.

[18] S. Lee, H. Kato, T. Kubota, K. Yubuta, A. Makino, A. Inoue, Excellent thermal stability and bulk glass forming ability of Fe-B-Nb-Y soft magnetic metallic glass, Mater. Trans. 49 (2008) 506–512.
[19] Q.K. Man, A. Inoue, Y.Q. Dong, J. Qiang, C.L. Zhang, B.L. Shen, A new CoFe-based bulk metallic with high thermoplastic forming ability, Scr. Mater. 69 (2013) 553–556.
[20] J.H. Yao, J.Q. Wang, Y. Li, Ductile Fe-Nb-B bulk metallic glass with ultrahigh strength, Appl. Phys. Lett. 92 (2008) 251906.
[21] F. Hu, Q. Luo, B.L. Shen, Thermal, magnetic and magnetocaloric properties of FeErNbB metallic glasses with high glass-forming ability, J. Non-Cryst. Solids 512 (2019) 184–188.
[22] J.W. Li, W.M. Yang, D. Estéve, G.X. Chen, W.G. Zhao, Q.K. Man, Y.Y. Zhao, Z.D. Zhang, B.L. Shen, Thermal stability, magnetic and mechanical properties of Fe-Dy-B-Nb bulk metallic glasses with high glass-forming ability, Intermetallics 46 (2014) 85–90.
[23] D. Ma, H. Tan, D. Wang, Y. Li, E. Ma, Strategy for pinpointing the best glass-forming alloys, Appl. Phys. Lett. 86 (2005) 191906.
[24] J. Zhou, B.A. Sun, Q.Q. Wang, Q.M. Yang, W.M. Yang, B.L. Shen, Effects of Ni and Si additions on mechanical properties and serrated flow behavior in FeMoPCB bulk metallic glasses, Journal of Alloys and Compounds, J. Alloy. Comp. 783 (2019) 555–564.
[25] W.H. Wang, Bulk metallic glasses with functional physical properties, Adv. Mater. 21 (2009) 4524–4544.
[26] W. Zhang, F. Jia, X.G. Zhang, G.Q. Xie, H. Kimura, A. Inoue, Two-stage-like glass transition and the glass-forming ability of a soft magnetic Fe-based glassy alloy, J. Appl. Phys. 105 (2009), 053518.
[27] S. Lan, Y. Ren, X.Y. Wei, B. Wang, E.P. Gilbert, T. Shibayama, S. Watanabe, M. Ohnuma, X.L. Wang, Hidden amorphous phase and reentrant supercooled liquid in Pd-Ni-P metallic glasses, Nat. Commun. 8 (2017) 14679.
[28] W.M. Yang, J.W. Li J, H.S. Liu, C.C. Dun, H.L. Zhang, J.T. Huo, L. Xue, Y.C. Zhao, B.L. Shen, L.M. Dou, A. Inoue, Origin of abnormal glass transition behavior in metallic glasses, Intermetallics 49 (2014) 52–56.
[29] G. Kumar, D. Nagahama, M. Ohnuma, T. Ohkubo, K. Hono, Structural evolution in the supercooled liquid of $Zr_{36}Ti_{24}Be_{40}$ metallic glass, Scr. Mater. 54 (2006) 801–805.
[30] J.H. Na, S.W. Sohn, W.T. Kim, D.H. Kim, Two-step-like anomalous glass transition behavior in Ni-Zr-Nb-Al-Ta metallic glass alloys, Scr. Mater. 57 (2007) 225–228.
[31] J.C. Ge, H.Y. He, J. Zhou, C.Y. Lu, W.X. Dong, S.N. Liu, S. Lan, Z.D. Wu, A.D. Wang, L. Wang, C. Yu, B.L. Shen, X.L. Wang, In-situ scattering study of a liquid-liquid phase transition in Fe-B-Nb-Y supercooled liquids and its correlation with glass-forming ability, J. Alloy. Comp. 787 (2019) 831–839.
[32] K. Zhao, X.X. Xia, H.Y. Bai, D.Q. Zhao, W.H. Wang, Room temperature homogeneous flow in a bulk metallic glass with low glass transition temperature, Appl. Phys. Lett. 98 (2011) 141913.
[33] J. Schroers, T.M. Hodges, G. Kumar, H. Raman, A.J. Barnes, P. Quoc, T.A. Waniuk, Thermoplastic blow molding of metals, Mater. Today 14 (2011) 14–19.
[34] J.W. Li, D. Estéveza, K.M. Jianga, W.M. Yang, Q.K. Man, C.T. Chang, X.M. Wang, Electronic-structure origin of the glass-forming ability and magnetic properties in Fe-RE-B-Nb bulk metallic glasses, J. Alloy. Comp. 617 (2014) 332–336.
[35] A. Chrobak, V. Nosenko, G. Haneczok, L. Boichyshyn, B. Kotur, A. Bajorek, O. Zivotsky, A. Hendrych, Effect of rare earth additions on magnetic properties of $Fe_{82}Nb_2B_{14}RE_2$ (RE= Y, Gd, Tb and Dy) amorphous alloys, Mater. Chem. Phys. 130 (2011) 603–608.
[36] H. Kato, N. Kurita, Y. Ando, T. Miyazaki, M. Motokawa, Magnetic properties of random-anisotropy amorphous magnets $(R_xFe_{1-x})_{80}Si_{12}B_8$ with R= Pr, Nd, Sm, Tb, Dy and Er, J. Magn. Magn. Mater. 189 (1998) 263–273.
[37] H. Kronmuller, Theory of the coercive field in amorphous ferromagnetic alloys, J. Magn. Magn. Mater. 24 (1981) 159.
[38] X.B. Liang, T. Kulik, J. Ferenc, M. Kowalczyk, G. Vlasak, W.S. Sun, B.S. Xu, Influence of structure on coercivity in nanocrystalline $(Fe_{1-x}Co_x)_{86}Hf_7B_6Cu_1$ alloys, Physica B 370 (2005) 151–157.
[39] J.W. Li, H. Men, B.L. Shen, Soft-ferromagnetic bulk glassy alloys with large magnetostriction and high glass-forming ability, AIP Adv. 1 (2011), 042110.
[40] M. Kersten, Problem der Technischen Mgnetisierungs Kurve, Springer, Berlin, 1938, p. 42.
[41] Z.Q. Liu, Z.F. Zhang, Mechanical properties of structural amorphous steels: intrinsic correlations, conflicts, and optimizing strategies, J. Appl. Phys. 114 (2013) 243519.